

S. Cvetkovski¹, L.P. Karjalainen¹, V. Kujanpää², A. Ahmad²

**WELDING HEAT INPUT DETERMINATION IN TIG AND LASER WELDING OF LDX 2101
STEEL BY IMPLEMENTING THE ADAMS EQUATION FOR 2-D HEAT DISTRIBUTION**
**ODREĐIVANJE UNOSA TOPLOTE ZA TIG I LASERSKO ZAVARIVANJE ČELIKA LDX 2101
UVOĐENJEM JEDNAČINE ADAMSA ZA 2-D RASPODELU TOPLOTE**

Original scientific paper
UDC: 621.791.7.01:536
Paper received: 10.11.2009

Author's address:
¹ University of Oulu, Department of Mechanical
Engineering, Box 4200, 90014 Oulu, Finland
² Lappeenranta University of Technology, 53851
Lappeenranta, Finland

Keywords

- TIG welding
- laser welding
- heat distribution
- thermal simulation
- duplex stainless steel

Abstract

The heat input applied in arc welding can be estimated based on the power of the welding power source and the thermal efficiency of the welding process. In laser welding, however, the absorption of laser beam can vary very significantly, so that the estimation of laser heat input is difficult. In the present paper a method is described to estimate the real heat input applied in welding based on the determination of the temperature distribution in a welded joint of a duplex stainless steel sheet. The temperature distribution is determined based on observations of the positions of certain metallurgical microstructures in the heat-affected zone. The exact temperatures for the formation of these specific microstructures were obtained by thermal simulation using various peak temperatures and cooling rates.

INTRODUCTION

In laser beam welding, the absorption of the beam in the metal is not generally known, so that the welding heat input cannot be calculated directly. The basic idea of this study is to develop a procedure for determination of heat input in the laser welding process by implementing the Adams equation for the two-dimensional heat distribution. To realize this idea, it is necessary to determine two character-

Ključne reči

- TIG zavarivanje
- lasersko zavarivanje
- raspodela toplote
- termička simulacija
- dupleks nerđajući čelici

Izvod

Unos toplote kod zavarivanja električnim lukom se može odrediti na osnovu snage izvora toplote za zavarivanje i iskorišćenja toplote datog postupka zavarivanja. Kod laserskog zavarivanja, međutim, apsorpcija laserskog snopa može da se menja u većoj meri, tako da je otežano određivanje unosa toplote laserom. U ovom radu opisan je metod za određivanje realnog unosa toplote kod zavarivanja na bazi određivanja temperaturne raspodele unutar zavarenog spoja u jednoj ploči od dupleks nerđajućeg čelika. Temperaturna raspodela se određuje na osnovu posmatranja lokacija pojedinih mikrostruktura u zoni uticaja toplote. Tačne temperature za formiranje ovih specifičnih mikrostruktura dobijene su termičkom simulacijom primenom raznih temperaturnih maksimuma i brzina hlađenja.

istic microstructure locations corresponding to the known peak temperatures in weld HAZ, and to measure the distance between them. Implementing the measured distance in the Adams equation, the absorption coefficient can be determined, and finally heat input can be calculated.

MATERIAL AND EXPERIMENT

LDX 2101 (EN 1.4162; UNS S32101) is quite a new duplex steel grade. It is a low-alloyed, general-purpose duplex stainless steel. The main properties of LDX 2101 steel are: high strength and fatigue resistance, very good weldability, high corrosion resistance and resistance to stress corrosion cracking and high energy absorption [1–7]. The balanced chemical composition of LDX 2101, given in Table 1, results in a microstructure containing approximately equal amounts of ferrite and austenite.

Table 1. Chemical composition of LDX2101 duplex stainless steel.
Tabela 1. Hemijski sastav dupleks nerđajućeg čelika LDX2101.

Element	C	N	Cr	Ni	Mo	Mn
wt. %	0.03	0.22	21.5	1.5	0.3	5.0

LDX 2101 steel sheets with the thickness of 3 mm were investigated in this study. The test material was provided by Outokumpu Stainless Oy (Tornio, Finland). Two autogenous, automatic TIG, bead-on-plate welding experiments were carried out. The welding parameters employed are given in Table 2. An intention was to obtain two-dimensional thermal conduction conditions, i.e. deep full penetration. In the present tests, typical cross-sections of the welds are shown in macro photos in Fig. 1.

Table 2. Welding parameters used in two autogenous TIG bead-on-plate welding experiments.

Tabela 2. Parametri zavarivanja upotrebljeni kod dva eksperimenta autogenog TIG zavarivanja ploče.

Parameters	Weld a	Weld b
Current (A)	120	150
Voltage (V)	12	12
Welding speed (mm/min)	220	250
Heat input Q (J/mm)	236	260

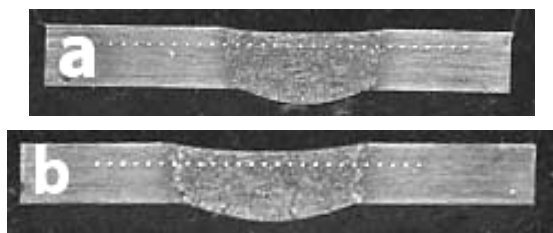


Figure 1. Macro photos of cross-sections of TIG welded joints.
Slika 1. Makro snimci preseka šava TIG zavarenih spojeva ploče.

Laser welding experiments were carried out at Lappeenranta University of Technology, employing CO₂ laser (He shielding gas with the flow rate of 20 l/min) in the keyhole mode. Applied parameters for laser welding tests are given in Table 3. Typical cross-sections are shown in Fig. 2.

Table 3. Welding parameters for laser welding tests.
Tabela 3. Parametri za ispitivanje laserskog zavarivanja.

Weld No.	Sheet thickness (mm)	Laser power (W)	Welding speed (m/min)	Focal length (mm)
13	3	5000	1	300
20	3	5000	4.5	300
33	3	5000	1.5	200
36	3	5000	6	200

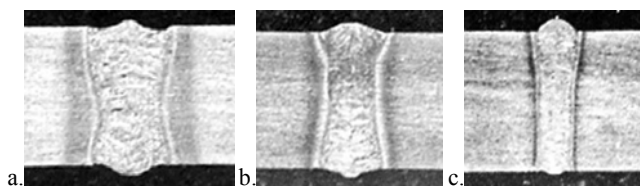


Figure 2. Macro photos of cross-sections of laser weldments
a) No 13 b) No 33 c) No 36
Slika 2. Makro snimci preseka šavova laserski zavarenih spojeva
a) No 13 b) No 33 c) No 36

Simulation of the influence of thermal heat input on HAZ microstructures was performed on a Gleeble 1500 simulator. The shape and dimensions of the specimens for simulation experiments are shown in Fig. 3. The following parameters were used in the simulation experiments:

- heating rate: 500 °C/s
- peak temperatures: 900, 1000, 1100, 1200, 1250, 1300 and 1350 °C/s
- holding time: 1 s
- cooling time, $\Delta t_{8/5}$: 1.7 s (air cooling), 5 s and 10 s.

Thermal history curves in the simulation experiments with the peak temperatures in the range 900–1350°C and the cooling time of 1.7 s (air cooling) can be seen in Fig. 4.

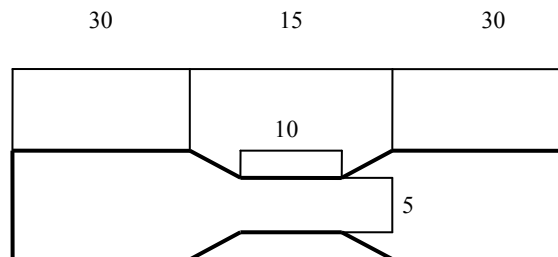


Figure 3. Shape and dimensions of specimens for thermal simulation.

Slika 3. Oblik i dimenzije epruveta za termičku simulaciju.

After the bead-on-plate TIG and laser welding experiments and the Gleeble simulation, hardness measurements and metallographic investigations were performed. Hardness (HV₂) was measured along the line beneath the surface of the sheet with the interval of 0.5 mm between the measuring points. Nine measurements were made on every specimen and the mean values were used.

Preparation of metallographic specimens

From simulated specimens, and TIG and laser weldments, specimens for metallographic investigations were made. Standard metallographic preparation of specimens was performed. Many trials with different electrolytic and chemical etchants were performed for appropriate revealing of characteristic microstructure. Quantitative and qualitative metallographic analysis was made using NIKON optical microscope.

RESULTS

The influence of the peak temperature and cooling rates on the hardness is shown in Fig. 5.

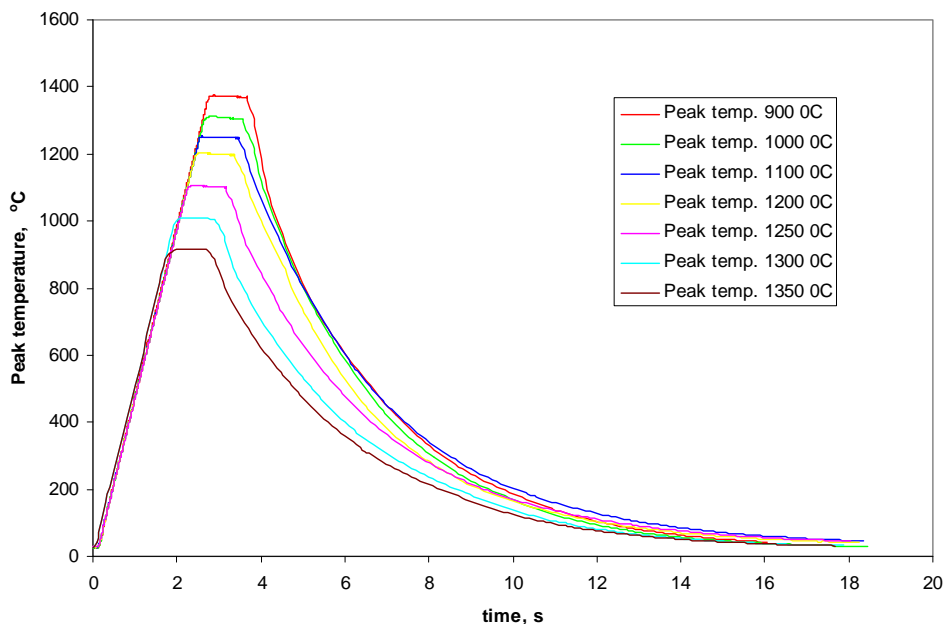


Figure 4. Thermal curves in simulation: heating rate 500°C/s, holding time 1 s, cooling time 1.7 s.
Slika 4. Termičke krive u simulaciji: brzina zagrevanja 500°C/s, vreme držanja 1s, vreme hlađenja 1.7 s.

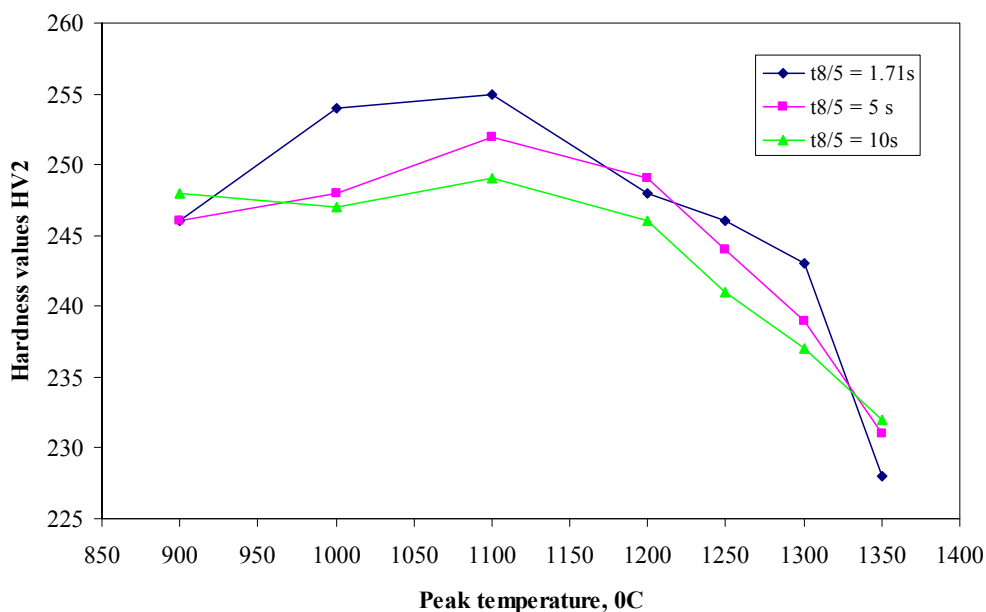


Figure 5. Hardness values vs. simulation peak temperature and cooling rate.
Slika 5. Vrednosti tvrdoće u zavisnosti od najveće temperature simulacije i brzine hlađenja.

Welding simulation – characteristic microstructural changes

Microstructures of specimens heated to peak temperatures in the range from 900 to 1350 °C and the cooling time of $\Delta t_{8/5} = 5$ s are shown in Fig. 6. Generally it can be seen that banded duplex ferritic-austenitic microstructure is dominant up to 1300 °C. With increasing peak temperature the width of the bands tended to increase. This is most obvious at the high peak temperatures of 1250 and 1300 °C. At 1300 °C, the banded structure is still present, but as seen in Fig. 6d, destruction of the banded structure starts at some isolated locations. At the temperature of 1350°C, completely retransformed microstructure is observed. New equi-

axed ferrite grains are formed with the austenite on grain boundaries and in some cases inside the grains (Fig. 6e).

Another observation from metallographic investigations of simulated specimens is the precipitation of particles, presumably chromium nitrides, inside the ferrite grains, appearing as dark or black spots. From analysis of Figs. 6a and 6b, one can see that the start temperature of precipitation is 1000 °C. This conclusion was confirmed using different etchants: H₂SO₄, HNO₃ and Beraha etchant. The specimens shown in Fig. 6 were etched with 10% oxalic acid (4 V, 60 s). At highest temperatures, precipitation becomes very pronounced, so that grains appear almost black.

Hence, as a result of metallographic investigation of the thermal-simulated specimens, two characteristic temperatures can be determined:

- 1350 °C – peak temperature at which retransformation of banded microstructure appears,
- 1000 °C – peak temperature at which precipitation as dark spot clusters is detected in the ferrite bands.

Simulation using different cooling times, i.e. $\Delta t_{8/5} = 1.7, 5$ and 10 s did not show any noticeable difference in the microstructure. However, as seen in Fig. 5, there is a small difference in hardness values depending on the cooling times. It can also be noticed that above the peak temperature of 1100 °C, there is slight drop in hardness, probably due to grain growth at higher temperatures.

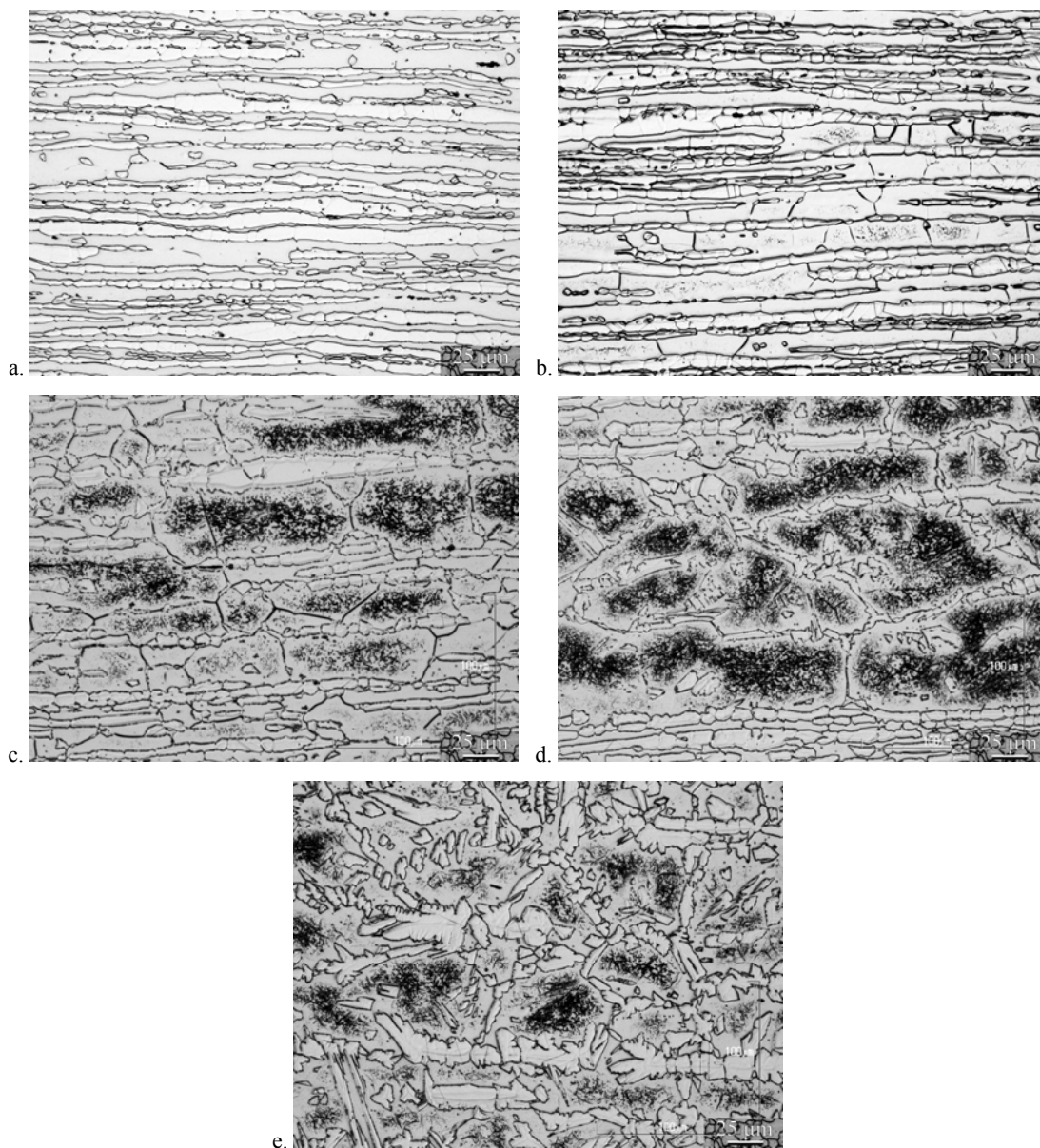


Figure 6. Microstructure of LDX 2101 steel in simulation thermal cycles with $\Delta t_{8/5} = 5$ s (etching in 10% oxalic acid).

Peak temperatures: a) 900 °C, b) 1000 °C, c) 1250 °C, d) 1300 °C, e) 1350 °C.

Slika 6. Mikrostrukture čelika LDX 2101 u simuliranim termičkim ciklusima sa $\Delta t_{8/5} = 5$ s (nagrizanje u 10% oksalna kiselina).

Maksimalne temperature: a) 900 °C, b) 1000 °C, c) 1250 °C, d) 1300 °C, e) 1350 °C.

Microstructure of TIG welded joints

Similar microstructures as in the thermal simulated specimens are detected in the HAZ of TIG welded joints, Fig. 7. In Figure 7a the start of precipitation can be noticed. In Figure 7b, the weld metal, fusion line and HAZ adjacent to the fusion line are shown. Retransformation of microstructure and formation of equiaxed ferrite grains with

austenite along grain boundaries and inside the grains are distinct. Precipitated particles are numerous, too.

Precipitates in the coarse-grained HAZ and weld metal can be seen in Fig. 8 at a higher magnification. Precipitation occurs both inside the grains and on interfaces of ferrite/austenite grains. However, it was realized that short-time etching, i.e. light, worked much better for precipitation analysis (oxalic acid, 4 V with 40 s etching time).

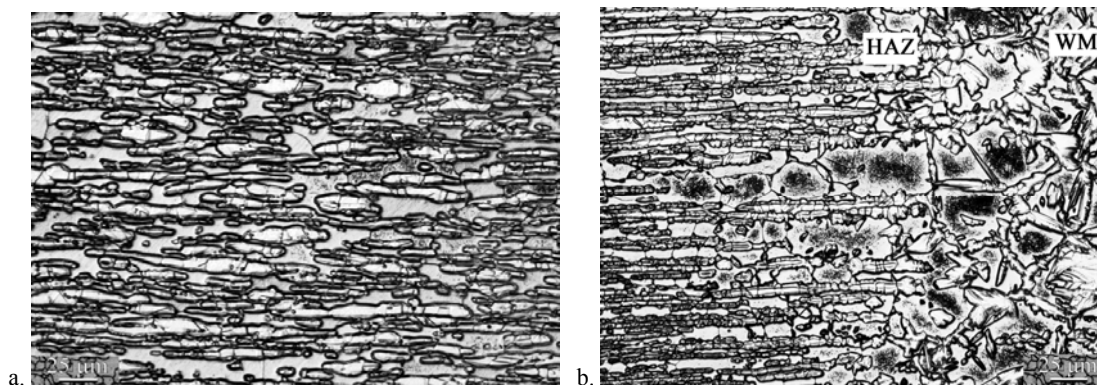


Figure 7. Microstructure of autogenous TIG bead-on-plate welded joint, $Q = 236 \text{ J/mm}$, a) start of precipitation, b) HAZ, fusion line and weld metal.

Slika 7. Mikrostruktura autogenog TIG zavarivanja ploče, $Q = 236 \text{ J/mm}$, a) početak taloženja, b) ZUT, linija stapanja i metal šava.

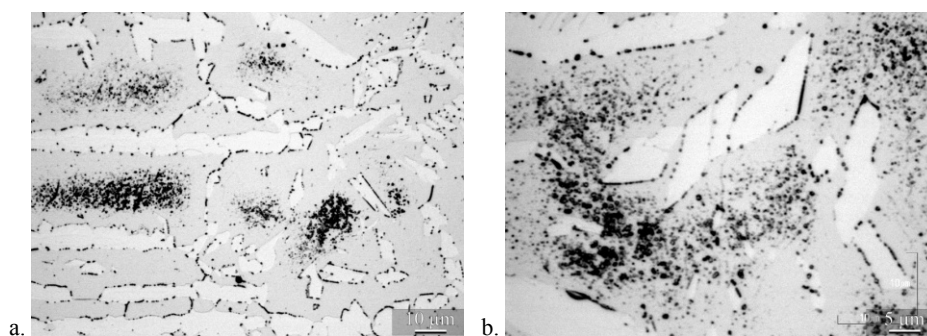


Figure 8. Precipitation in TIG bead-on-plate weldments, a) HAZ, b) weld metal.

Slika 8. Taloženje u TIG zavarenom spoju, a) ZUT, b) metal šava.

Metallographic investigations of laser weldments

From macro-photos in Figure 2, a difference in the width of the weld metal and HAZ can be ascertained as a result of different heat inputs. Besides, in the weld No 36 with the lowest laser power applied, there is much more intensive

precipitation of particles in the weld metal than in other weldments, Fig. 9. As a result of high cooling rate due to low heat input, there is much more ferrite in the weld metal microstructure and adjacent to the fusion line. From pre-saturated ferrite, heavy precipitation of particles can occur.

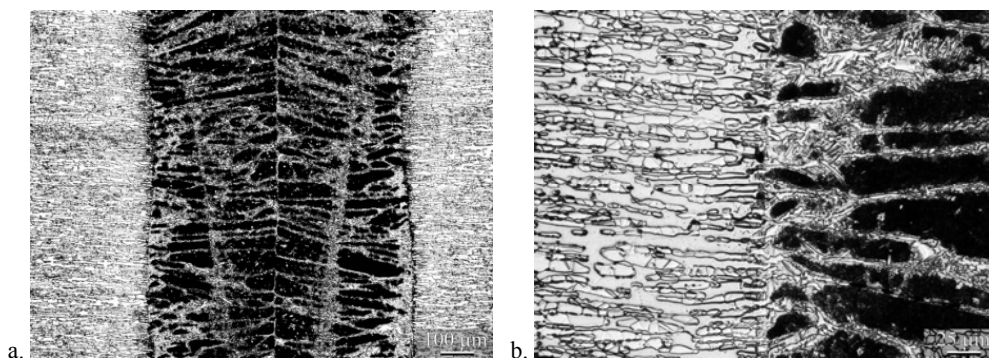


Figure 9. Microstructure of laser weldment, test No 36, a) weld metal – low magnification b) HAZ, fusion line and weld metal.

Slika 9. Mikrostrukture laserski zavarenog spoja, uzorak No 36, a) metal šava – malo uvećanje, b) ZUT, linija stapanja i metal šava.

Another observation is that there is not such characteristic microstructure of the high temperature HAZ in laser weldments as was found in TIG weldments. The equiaxed grains could not be seen, but only banded ferrite and austenite even very close to the fusion line. However, there is a sharp fusion line between the weld metal and HAZ, as obvious in Fig. 9b, that displays the microstructure of the weld No 36.

Determination of welding heat input using Adams equation and comparing to heat input applied in TIG welding

After metallographic analysis of simulated specimens and autogenous TIG bead-on-plate welded joints, the procedure for heat input determination using the Adams equation was performed. As previously pointed out, two characteristic peak temperatures (T_p) could be observed in welding simulation:

- 1350°C – temperature of microstructural retransformation,
- 1000°C – start temperature of nitride particle precipitation.

However, the higher temperature could not be seen in laser welds, the fusion line, i.e. the melting temperature (T_m) of 1445°C, the value taken from literature [8], was used in the calculations.

The heat input in TIG bead-on-plate welding was determined using a well-known equation for arc welding. The values of the parameters were given in Table 2.

$$Q = \eta \frac{U \cdot I \cdot 60}{v \cdot 1000} \quad (\text{kJ/mm}) \quad (1)$$

where: U –voltage (V); I –current (A); v –welding speed (mm/min); η –efficiency of the welding process.

Calculated values for Q from equation (1) were implemented in the Adams equation in order to determine the distance between the fusion line and the precipitation start

location (1000°C). The Adams equation (2) for the 2D-temperature distribution is as follows:

$$\frac{1}{T_p - T_0} = \frac{4.13 \cdot \rho \cdot t \cdot c \cdot Y}{Q} + \frac{1}{T_m - T_0} \quad (2)$$

The parameters and their values used for LDX 2101 steel are the following: density of material, $\rho = 0.008 \text{ g/mm}^3$; thickness of sheet, $t = 3 \text{ mm}$; specific heat capacity, $c = 0.5 \text{ J/g}^\circ\text{C}$; Y = distance between two temperature points (mm); melting temperature, $T_m = 1445^\circ\text{C}$; ambient temperature $T_0 = 20^\circ\text{C}$; peak temperature, $T_p = 1000^\circ\text{C}$; heat input Q (J/mm).

Using a NIKON optical microscope, the corresponding distance was determined by direct measurement. In Figure 10, the measurement using optical microscopy has been demonstrated. The values for the distance from measurements and calculations are given in Table 4.

Table 4. Measured and calculated values for the distance between 1445 and 1000 °C.

Tabela 4. Izmerene i sračunate vrednosti za rastojanje između 1445 i 1000 °C.

Temperature	TIG a, $Q = 236 \text{ J/mm}$		TIG b, $Q = 260 \text{ J/mm}$	
Distance (μm)	Measured	Calculated	Measured	Calculated
1445/1000 °C	1472	1517	1629	1672

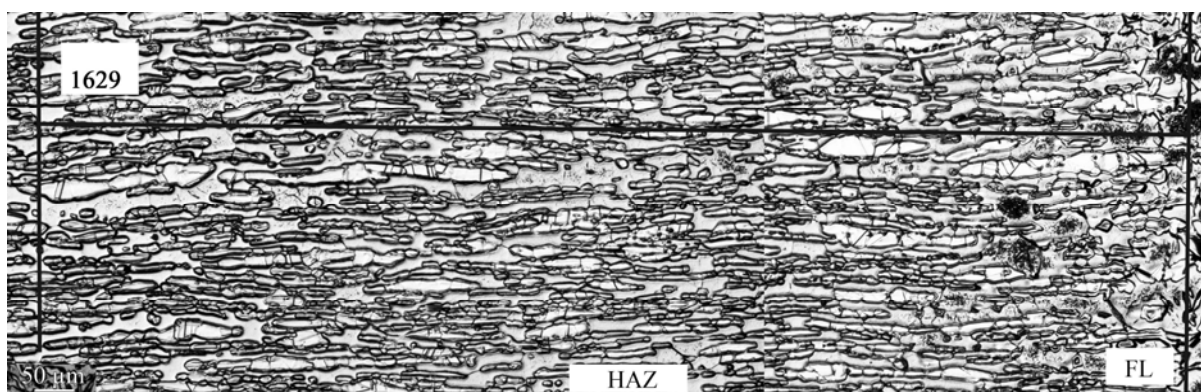


Figure 10. Determination of the distance 1445/1000°C for the TIG weldments with $Q = 260 \text{ J/mm}$.

Slika 10. Određivanje rastojanja 1445/1000°C za TIG zavarene spojeve sa $Q = 260 \text{ J/mm}$.

As seen, the procedure shows very good consistence between the measured and calculated values for TIG welding, so that it can be implemented for laser welding, too.

Determination of welding heat input using the Adams equation in laser welding

Similarly as for TIG welds, from metallographic photos, the distance between the fusion line and precipitation start location, i.e. 1445/1000°C, could be obtained for laser welds, too. These values are implemented in the Adams equation (2) to predict the heat input. From this, using the

known laser power in the experiment, the efficiency factor, i.e. the absorption coefficient can be calculated (eq. (1)).

Determination of the distance 1445/1000 °C in the case of different laser weldments is illustrated in Figs. 11 and 12, and the values obtained for the absorption are listed in Table 5. Typical considerable scatter in results is demonstrated for weld No 36 in Fig. 12, due to position of the measurement; near upper or lower surface, for instance. Through thickness variation of the shape of weld metal is evident in Figure 2.

Table 5. Absorption values obtained in laser welding and the parameters used in its calculation.

Tabela 5. Vrednosti apsorpcije dobijene kod laserskog zavarivanja i parametri upotrebljeni za proračun.

Laser weld No	Laser power (W)	Welding speed (mm/min)	Distance (μm)	Absorption, %
13	5000	1000	612	32
33	5000	1500	375	29
36	5000	6000	113	35
36	5000	6000	144	44

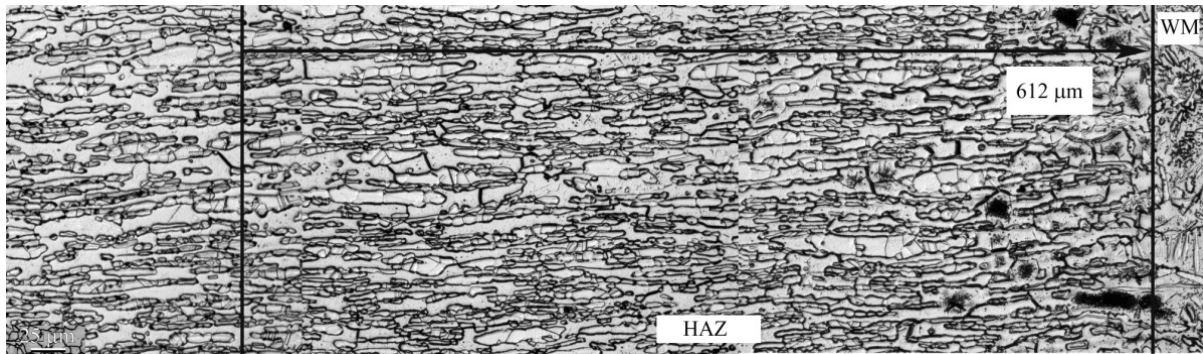


Figure 11. Determination of the distance between temperatures 1445 and 1000°C from the microstructure seen in optical microscope. Laser weld specimen No 13.

Slika 11. Određivanje rastojanja između temperatura 1445 i 1000°C iz mikrostrukture na optičkom mikroskopu. Laserski zavareni uzorak No 13.

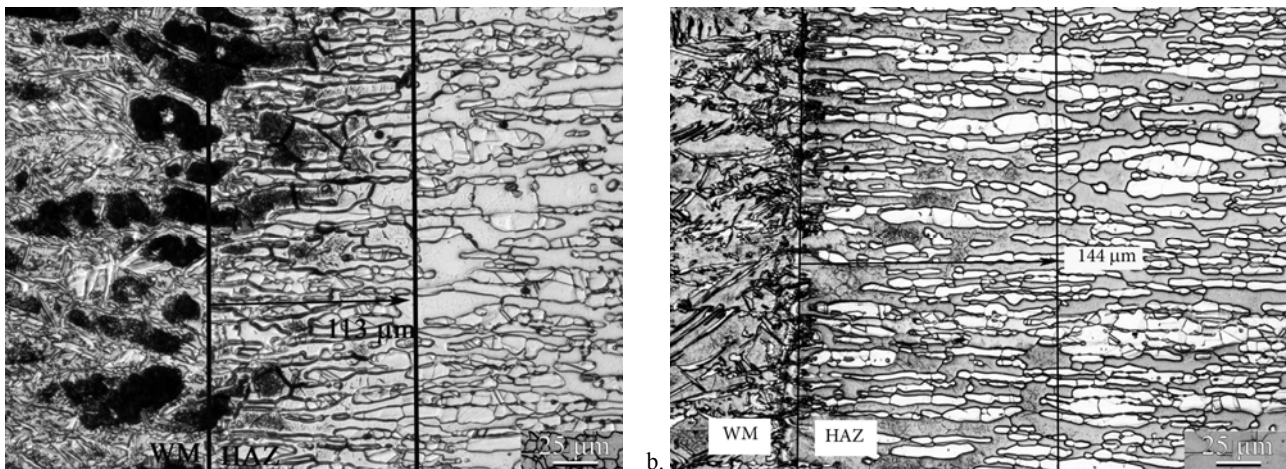


Figure 12. Determination of the distance between temperatures 1445 and 1000°C from the microstructure seen in optical microscope. Laser weld specimen No 36, a) absorption 35%, b) absorption 44%.

Slika 12. Određivanje rastojanja između temperatura 1445 i 1000°C iz mikrostrukture na optičkom mikroskopu. Laserski zavareni uzorak No 36, a) apsorpcija 35%, b) apsorpcija 44%.

CONCLUSION

For LDX 2101 duplex stainless steel, thermal simulation indicated that two characteristic temperatures can be determined from the microstructure:

- 1350°C – the peak temperature at which retransformation of banded duplex microstructure appears. New equiaxed ferrite grains delineated with austenite and smaller amount of austenite inside the grains are formed.
- 1000°C – the lowest peak temperature at which precipitation of particles, presumably chromium nitrides, with appearance of dark spot clusters can be discovered in optical microscope in the ferrite bands. This temperature was used in the calculations performed.

Based on the measured distances between the fusion line and the location of precipitation start, the heat input was calculated by the Adams equation for autogenous bead-on-plate TIG welds and found to be consistent with the real heat inputs applied in the experiments.

For CO₂ – laser welds, the same procedure was adopted. The absorption coefficients obtained varied between 29 and 44 %, local variation being pronounced, too.

ACKNOWLEDGEMENT

The experimental material LDX 2101 was supplied by Outokumpu Stainless Oy. The funding from The Finnish Funding Agency for Technology and Innovation, Outokumpu Oyj, Rautaruukki Oyj and Metso Paper Oy is acknowledged with gratitude in the project “Laser Heat” 40175/08 (Dnro 799/31/08).

REFERENCES

1. LDX 2101 Duplex Stainless, Outokumpu Stainless AB
2. DATA SHEET LDX 2101 UNS S32101, Outokumpu Stainless
3. Ralph Davison, LDX New, Cost Effective Stainless Steel, Outokumpu Stainless
4. James Chater, *The best of most worlds: recent developments in duplex and super duplex alloys*, url: www.stainless-steel-world.net
5. Anders Olsson, Market and Trends – Stainless Steel, Outokumpu Stainless AB
6. LDX 2101 Comparative to last, Outokumpu Stainless
7. LDX 2101 AC/DC Covered electrodes url: www.avestawelding.com
8. Corrosion resistant rolled alloys, url: www.RolledAlloys.com